# COORDINATED UV AND OPTICAL OBSERVATIONS OF THE AM HERCULIS OBJECT E1405−451 IN THE HIGH AND LOW STATES[1]

L. MARASCHI AND A. TREVES
Dipartimento di Fisica, Università di Milano

E. G. TANZI
Istituto di Fisica Cosmica, CNR, Milano

M. MOUCHET AND A. LAUBERTS
European Southern Observatory

C. MOTCH
Observatoire de Besançon

J. M. BONNET BIDAUD
C. E. A. Section d'Astrophysique, Saclay

AND

M. M. PHILLIPS
Cerro Tololo Inter-American Observatory[2]

## ABSTRACT

Simultaneous UV and optical observations of the magnetic white dwarf binary E1405−451 taken in 1983 February, March, and April are reported. In March the source was found in a low state analogous to those observed in AM Her. In this state the ultraviolet spectrum of E1405−451 can be interpreted as the emission from a hot white dwarf [$T = 26,500$ K, $R = 3 \times 10^8 \times (d/100$ pc) cm], and the $R$ and $I$ magnitudes can be accounted for by a Roche lobe filling secondary, of spectral type between M3 V and M8 V at a distance between 50 and 200 pc. Emission from a residual accretion column may still be present. In the high state, the UV continuum is described by a power law $F_\lambda \propto \lambda^{-\alpha}$ with $\alpha = 1.9$, while the optical and infrared magnitudes lie above the extrapolation of this power law. Subtracting the emission of the white dwarf and of the secondary from the overall energy distribution in the high state, the residual spectrum seems to contain two components. A steep one, emerging shortward of 2000 Å, could be associated with a hot polar cap, ($F_\lambda \propto \lambda^{-4}$), a flatter one, $F_\lambda \propto \lambda^{-1}$, between 2000 and 6000 Å, rapidly decreasing in the infrared, could be due to cyclotron radiation.

*Subject headings:* radiation mechanisms — stars: binaries — stars: individual — stars: magnetic — stars: white dwarfs — ultraviolet: spectra

## I. INTRODUCTION

The X-ray source E1405−451 = H1405−45 was recently identified with a blue star with emission lines (Jensen, Nousek, and Nugent 1982; Mason *et al.* 1983). Optical photometry (Mason *et al.* 1983) revealed a rather complex light curve, with a 101.5 m periodicity, with a maximum to minimum modulation of ~1 mag. The presence of linear and circular, phase-dependent, polarization (Tapia 1982; Bailey *et al.* 1983; Visvanathan and Tuohy 1983) showed that the object is an AM Her type variable (e.g., Chiappetti, Tanzi, and Treves 1980; Wickramasinghe 1982; Liebert and Stockman 1983). The ultraviolet spectrum observed by Nousek and Pravdo (1983) is also similar to that observed in AM Her type binaries.

Here we report on three sets of coordinated *IUE* and ground-based observations of the source obtained in 1983 February, March, and April. A journal of the observations is given in Table 1. Phases were computed using the following ephem-

eris (S. Tapia, private communication): $T_{min} = $ JDH 2,445,048.9433(2) + $N \times 0^d07049598(8)$, where phase 0 corresponds to the minimum in the circular polarization and in the light curve.

While in February and April the source was in a state similar to that of 1982 January (Nousek and Pravdo 1983) and 1981 June (Mason *et al.* 1983), in March it was considerably fainter ($\Delta m \sim 1$ mag), both at optical and UV frequencies, and the emission lines almost disappeared.

## II. UV OBSERVATIONS

The UV spectra were obtained with the *International Ultraviolet Explorer* using short and long wavelength cameras (Table 1). The faintness of the object did not allow us to obtain phase-resolved spectra. Therefore, exposure times of the order of the orbital period were typically chosen. The object was acquired in the large aperture of the spectrograph (10 × 20 oval) by means of the standard offset technique with coordinates

$$\alpha_{1950} = 14^h05^m58^s2 , \quad \delta_{1950} = -45°03'04''6 ,$$

as measured on the glass copy of the ESO sky survey. The images were analyzed with the procedure developed at ESO,

214

TABLE 1

JOURNAL OF OBSERVATIONS

| Instrumentation | Spectrum Identification | Wavelength Interval | Time of Midexposure | Exposure Length (minutes) | Orbital Phase at Midexposure |
|---|---|---|---|---|---|
| | | 1983 February | | | |
| IUE ........................ | SWP 18269 | 1200–1900 | Feb 16 UT 7:22 | 18 | 0.75 |
| | LWR 15301 | 2000–3100 | Feb 16 UT 8:24 | 97 | 0.36 |
| | SWP 19270 | 1200–1900 | Feb 16 UT 10:57 | 200 | 0.86 |
| | LWR 15302 | 2000–3100 | Feb 16 UT 13:18 | 52 | 0.26 |
| 1.5 m CTIO (SIT + Vidicon) ......... | 16036 | | Feb 16 UT 7:31 | 20 | 0.83 |
| | 16037 | | Feb 16 UT 7:53 | 20 | 0.05 |
| | 16038 | 4000–7000 | Feb 16 UT 8:17 | 20 | 0.29 |
| | 16039 | | Feb 16 UT 8:36 | 15 | 0.47 |
| | 16040 | | Feb 16 UT 8:53 | 15 | 0.64 |
| | | 1983 March | | | |
| IUE ........................ | SWP 19359 | 1200–1900 | Mar 1 UT 6:24 | 40 | 0.59 |
| | | | Mar 1 UT 9:39 | 128 | 0.52 |
| IUE ........................ | LWP 1817 | 2000–3100 | Mar 1 UT 7:39 | 100 | 0.33 |
| 3.6 m ESO (IDS) .......... | ... | 4000–5900 | Mar 9 UT 9:42 | 5 | 0.04 |
| | | | Mar 9 UT 9:47 | 5 | 0.10 |
| 4 m CTIO (SIT + Vidicon) ......... | ... | 4300–5100 | Mar 10 UT 9:09 | 10 | 0.90 |
| 1 m ESO ................... | Photometry | $U$–$B$–$V$–$R_c$–$I_c$ | Mar 13 UT 8:03 | 12 | 0.82 |
| | | | Mar 13 UT 8:16 | 12 | 0.93 |
| | | | Mar 13 UT 8:28 | 12 | 0.08 |
| | | 1983 April | | | |
| IUE ........................ | SWP 19818 | 1200–1900 | Apr 26 UT 3:41 | 101 | 0.40 |
| | LWR 15818 | 2000–3100 | Apr 26 UT 5:02 | 51 | 0.21 |
| | SWP 19819 | 1200–1900 | Apr 26 UT 6:27 | 101 | 0.05 |
| 1, 5 m DANISH ESO ..... | Photometry | $BVI_c$ | Apr 26 UT 5:00 | 101 | 0.18 |
| 3, 6 m ESO ............... | Photometry | $JHK$ | Apr 26 UT 5:00 | 101 | 0.18 |

using the calibration curves reported in Bohlin and Holm (1981) and in Blades and Cassatella (1982). The short-wavelength spectra (1200–1900 Å) obtained on February 16, March 1, and April 26, are shown in Figure 1. The March spectrum differs substantially from the other two: emission lines are almost absent, the continuum intensity is lower and tends to decrease rather than increase toward shorter wavelengths.

### a) The Continuum

Average fluxes in selected wavelength intervals 50 Å wide, chosen to avoid strong lines and camera defects, were computed in order to study the continuum. The associated errors were assumed to be given by the standard deviation of the mean within the 50 Å band. The UV spectra taken earlier by Nousek and Pravdo (1983) were also reanalyzed in order to allow direct comparison with the 1983 data.

The continua measured on the same day do not differ significantly and were therefore combined in order to improve the signal-to-noise ratio. No absorption dip appears around 2200 Å in the 1983 data. A two-parameter fit with either a power law or a blackbody distribution gives only an upper limit of $E(B-V) \lesssim 0.15$ at the 95% confidence level. However, in the Nousek and Pravdo (1983) data the 2200 Å absorption feature is apparent, and the quality of the fits of these data improves significantly for $E(B-V) = 0.1$. In the following we shall therefore adopt this value of the reddening.

Table 2 gives, for the different epochs, broad-band fluxes in selected wavelength intervals and the best fit parameters of power-law and blackbody distributions with the corresponding reduced $\chi^2$. In all cases, except in the low state (1983 March), the power law fits better than the blackbody. The continua in 1983 February and April are 20% lower than in 1982 January, with a similar value of the spectral index $\alpha = 1.9$. In the low state a blackbody distribution with $T = 26,500$ K is clearly preferable to a power law.

### b) The Line Spectrum

The equivalent widths and intensities of the ultraviolet lines in the high state at different epochs are reported in Table 3. The profile of C IV $\lambda$1550 clearly shows a narrow unresolved component with broad wings of 40 Å FWZI. Significant intensity variations are observed not unequivocally related to the continuum intensity. In fact, the lines appear significantly weaker in 1983 February than in 1983 April, while the continua do not differ appreciably. On the other hand, in 1982 January, the continuum is 20% higher than in 1983 April, while the equivalent width of Si IV + O IV $\lambda$1400 is a factor of 3 larger; C IV $\lambda$1500 is 20% stronger, while all other lines appear comparable.

In the low state of 1983 March, the emission lines are strikingly weaker than in all other spectra. A complex feature seems to be present between 1500 and 1570 Å which could be interpreted as due to very broad C IV emission with two absorption dips at 1515 Å and 1550 Å, where two emission peaks were previously present (Nousek and Pravdo 1983). The equivalent width of C IV $\lambda$1550 is reduced by more than a factor 10, while the continuum faded by a factor 2. On the other hand, the
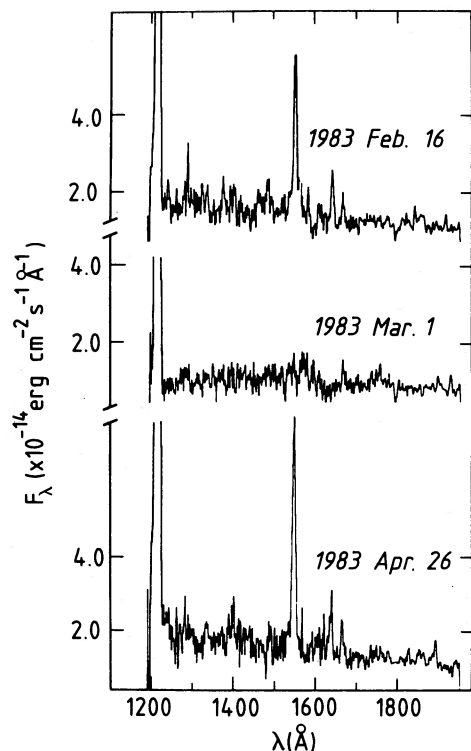
FIG. 1.—UV spectra of E1405−451. The March 1 spectrum corresponds to the low state of the source.

equivalent width of O III λ1660 appears similar to that in the high state.

### III. OPTICAL AND IR OBSERVATIONS

Optical observations were obtained simultaneously with the UV exposures in February (spectrophotometry) and April (optical and IR photometry). In March, photometric and spectroscopic information was provided 10 days after the UV observations (see Table 1).

On February 16 a full orbital period was covered with five exposures of 20 min using a SIT Vidicon detector at the Cassegrain spectrograph of the 1.5 m telescope of CTIO. A slit width of 3″7 was employed, giving a spectral resolution of 8.5 Å

(FWHM). The photometric accuracy of the calibration for these observations was verified to be of the order of 3%. Large variations in intensity of both continuum and lines were observed. The shape of the continuum is also variable with orbital phase.

In Figure 2, two spectra, corresponding respectively to maximum and minimum intensity, are shown. Emission lines of H I and He I, II are present. Average equivalent widths are given in Table 3. They are smaller by a factor 2 than those found by Mason *et al.* (1983), in 1981 June. It is also worth noting that the He II λ4686 in the February 16 spectra is considerably weaker, relative to the He I and H I lines, than was the case in the Mason *et al.* (1983) observations, indicating a generally lower level of ionization. Although the SIT Vidicon data are of only moderate spectral resolution, it is clear that the profiles of the emission lines, especially the Balmer series, change considerably through a period. An examination of the shape of Hβ (see Fig. 3) indicates that it is complex, with a broad component which seems to be rapidly variable. A red asymmetry is clearly present at phase 0.29 and a blue one at phases 0.47 and 0.64. At phase 0.05, the line appears to be narrower than at all other phases.

In Figure 4, the continuum intensity in selected bands and the intensity and equivalent widths of some Balmer lines are plotted versus phase. The minimum in the light curve appears less prominent at shorter wavelengths. The line intensities vary in accordince with the continuum, though with a smaller amplitude and a more sinusoidal shape. In fact, the equivalent widths show a maximum at phase 0.0.

Radial velocities of the peaks of the Hγ, Hβ, and Hα emission lines are plotted as a function of phase in Figure 5. Systematic variations are observed with a total amplitude of 500 km s⁻¹, which is comparable to the amplitude of the radial velocity variations seen in AM Her (Cowley and Crampton 1977) and other polars (Liebert and Stockman 1983). The derived mass function is 0.12 $M_\odot$. Zero velocity in E1405−451 apparently occurs near phases 0.0 and 0.5, which is not the case for any of the components of the emission lines in AM Her–like systems (cf. Liebert and Stockman 1983). Time-resolved spectra of E1405−451 at much higher resolution should be obtained in order to distinguish the motion of the regions emitting the broad and narrow components of the lines.

On March 9 and 10 two spectra were obtained with the 3.6

TABLE 2

UV FLUXES AND BEST FIT PARAMETERS

| EPOCH of OBSERVATION (1983) | SPECTRUM ID | $F_\lambda$ ($\times 10^{-14}$ ergs cm$^{-2}$ s$^{-1}$ Å$^{-1}$)[a] | | | | BEST FIT PARAMETERS[b] ($E_{B-V} = 0.1$) | | | | | |
|---|---|---|---|---|---|---|---|---|---|---|---|
| | | 1450 | 1750 | 2500 | 3000 | $K$ | $\alpha$ | $\chi^2$ | $A$ | $T$ | $\chi^2$ |
| Jan 3 ............... | {SWP 15943<br>{LWR 12273 | 1.62 | 1.39 | 0.66 | 0.55 | $6.1 \times 10^{-8}$ | 1.96 | 2.1 | $2.6 \times 10^{-24}$ | 26300 | 5 |
| Feb 16 ............. | {SWP 19270<br>{LWR 15301<br>{LWR 15302 | 1.42 | 1.00 | 0.51 | 0.43 | $2.9 \times 10^{-8}$ | 1.89 | 6.8 | $1.8 \times 10^{-24}$ | 28000 | 8.8 |
| Mar 1 ............... | {SWP 19359<br>{LWR 1817 | 0.81 | 0.84 | 0.37 | 0.22 | $1.1 \times 10^{-8}$ | 1.84 | 9.3 | $1.2 \times 10^{-24}$ | 26470 | 5.3 |
| Apr 26 ............. | {SWP 19818<br>{SWP 19819<br>{LWR 15818 | 1.46 | 1.06 | 0.55 | 0.48 | $4.1 \times 10^{-8}$ | 1.94 | 3.8 | $1.3 \times 10^{-24}$ | 30650 | 5.2 |

[a] Fluxes are averaged over 50 Å intervals. Errors, defined as standard deviation of the mean, are typically 5%. The photometric accuracy of *IUE* is better than 10%.

[b] Spectra have been fitted with power laws ($F_\lambda = K\lambda^{-\alpha}$) and blackbody distributions. For the latter case the given constant $A$ is the square of the ratio between the radius and the distance of the source.

TABLE 3
EMISSION LINES

| ID | (Å) | 1981 JUNE E.W. (Å) | 1982 JANUARY | | 1983 FEBRUARY | | 1983 APRIL | |
|---|---|---|---|---|---|---|---|---|
| | | | E.W. (Å) | $I$ ($10^{-14}$ ergs cm$^{-2}$ s$^{-1}$) | E.W. (Å) | $I$ ($10^{-14}$ ergs cm$^{-2}$ s$^{-1}$) | E.W. (Å) | $I$ ($10^{-14}$ ergs cm$^{-2}$ s$^{-1}$) |
| N v | 1240 | ... | 9 | 15 | 4 | 5 | 10 | 13 |
| C ii | 1336 | ... | 6 | 9 | 4 | 5 | 7 | 9 |
| Si iv + O iv | 1400 | ... | 47 | 79 | 14 | 18 | 17 | 20 |
| C iv | 1550 | ... | 96 | 135 | 53 | 59 | 80 | 80 |
| He ii | 1640 | ... | 20 | 26 | 11 | 12 | 18 | 17 |
| O iii | 1662 | ... | 4 | 5 | 4 | 5 | 11 | 10 |
| Al iii | 1860 | ... | 9 | 11 | 5 | 5 | 5 | 5 |
| Mg ii | 2800 | ... | 24 | 14 | 20 | 8 | 27 | 11 |
| Hγ | 4340 | 29 | ... | ... | 13 | 4 | ... | ... |
| He i | 4471 | 9 | ... | ... | 4 | 1 | ... | ... |
| He ii | 4686 | 26 | ... | ... | 5 | 2 | ... | ... |
| Hβ | 4861 | 50 | ... | ... | 20 | 6 | ... | ... |
| He i | 5876 | 9 | ... | ... | 6 | 1 | ... | ... |
| Hα | 6563 | 21 | ... | ... | 20 | 4 | ... | ... |

FIG. 2.—Optical spectra of E1405 − 451 on 1983 February 16 (high state) at two different phases
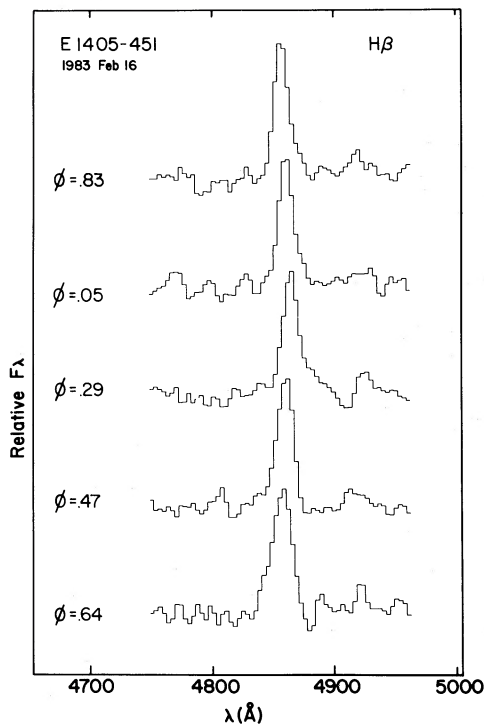


FIG. 3.—Profiles of Hβ at different phases (1983 Feb 16)

m telescope at ESO (courtesy of A. Ardeberg) and with the 4 m telescope at CTIO. They are shown in Figure 6. The photometric accuracy of these data is poor due to imperfect seeing conditions. Moreover, instabilities up to 7% in the response curve of the IDS used at the 3.6 m ESO telescope were observed. The weakness of the lines, compared to the February spectra, indicates a variation in equivalent width of more than a factor 10. In the CTIO spectrum, taken at orbital phase 0.8, Hγ and Hβ in emission are both weakly visible, while they are absent in the ESO spectrum, which was taken near phase 0. Absorption features seem to be present in both spectra with no obvious identifications. Some similarities with the spectrum of AM Her in low state (Schmidt, Stockman, and Margon 1981) suggest a possible interpretation of the features marked in the figure as Zeeman components of Hβ in absorption. If one associates the troughs around 4700, 4800, and 4900 Å with the three main components of Zeeman-split Hβ, using the curves computed by Angel (1977), a field between 10–15 megagauss is inferred.

Optical photometry ($UBVRI$) was obtained on March 13 with the 1 m ESO telescope at La Silla at phase $0.82 \leq \varphi \leq 0.08$. A modulation of 0.3 mag in $V$, $R$, $I$ was observed, while the $U$ and $B$ fluxes were constant. Magnitudes are given in Table 4.

On April 26 optical and IR photometry covering a full orbital period simultaneous with the $IUE$ exposures was obtained with the 1.5 m Danish and the 3.6 m telescopes at
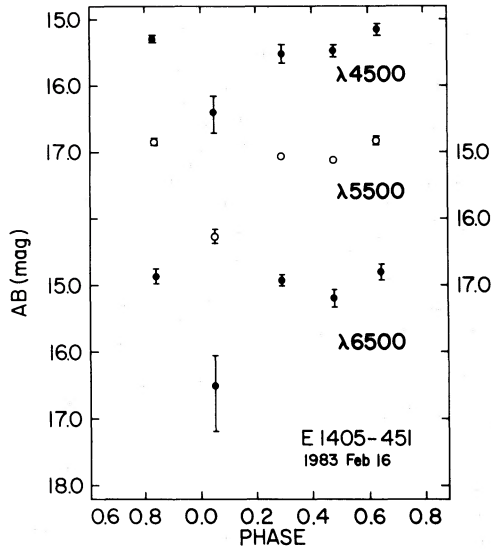
FIG. 4a
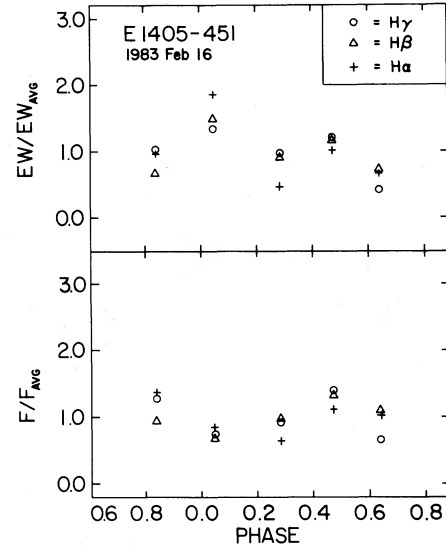


FIG. 4b

FIG. 4.—Data of 1983 February 16 (high state). (a) Broad-band fluxes at different wavelengths vs. phase. (b) (top) Equivalent width of Balmer lines normalized to the average value vs. phase. (bottom) Intensity of Balmer lines normalized to the average value vs. phase.

ESO La Silla. Light curves in B, V, $I_c$, and JHK were derived and will be presented in a separate paper. Average magnitudes to be compared with the UV continuum are given in Table 4.

### IV. DISCUSSION

Although the observations of E1405−451 cover a rather limited period, it appears that one can distinguish a two-state behavior similar to that of AM Her and of other polars. A low state occurred in 1983 March, lasting about two weeks. In this state, at orbital phase 0.8 (i.e., outside the minimum) $m_V = 16.6$, and the average ultraviolet flux is $F_{1500} = 8 \times 10^{-16}$ ergs cm$^{-2}$ s$^{-1}$ Å$^{-1}$. In the low state the ultraviolet lines, except O III $\lambda1660$, disappear, and the Balmer lines are weaker by more than a factor 10 in equivalent width.

### a) Low State Continuum

The low state spectrum can be used to deconvolve the contributions of various sources of light in the system.

The fact that the fit to the UV continuum with a blackbody distribution is considerably better than that with a power law, suggests an interpretation as emission from a white dwarf, in
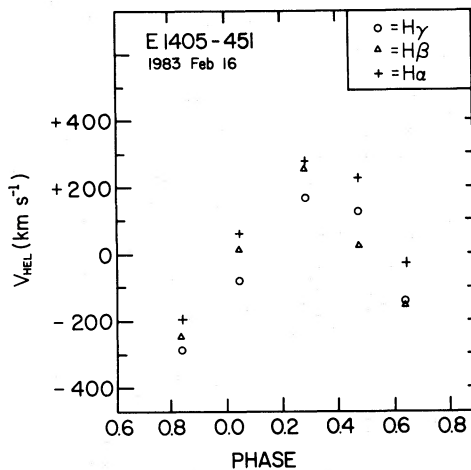


FIG. 5
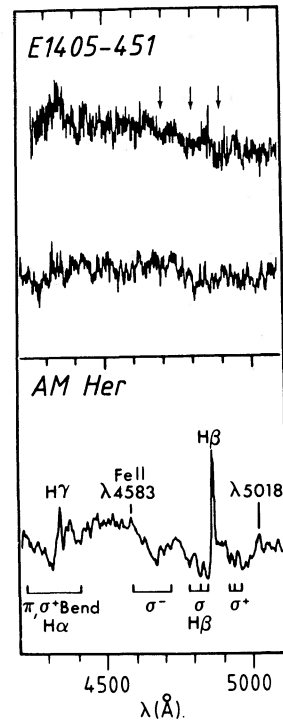


FIG. 6

FIG. 5.—Velocity vs. phase as deduced from the peak emission of the Balmer lines (1983 Feb 16)

FIG. 6.—Optical spectra of E1405−451 in low state (1983 March 9, 10). The upper spectrum was taken at CTIO; the lower one, at ESO. The ordinate scale is arbitrary. Arrows indicate the location of possible Zeeman components of Hβ. In the low frame the low state spectrum of AM Her observed by Schmidt *et al.* (1981) is included for comparison.

TABLE 4

OPTICAL AND INFRARED PHOTOMETRY AT
DIFFERENT EPOCHS

A. MARCH 13

| $\Phi$ | $U$ | $B$ | $V$ | $R_c$ | $I_c$ |
|------|------|------|------|------|------|
| 0.82 | 16.05 | 16.92 | 16.61 | 16.57 | 15.78 |
| 0.93 | 15.91 | 16.89 | 16.80 | 16.79 | 16.06 |
| 0.08 | 16.00 | 16.87 | 16.93 | 16.83 | 16.05 |

B. APRIL 26
TYPICAL AVERAGE OVER LIGHT CURVE

| $B^a$ | $V^a$ | $I_c{}^a$ | $J$ | $H$ | $K$ |
|------|------|------|------|------|------|
| 16.08 | 15.47 | 14.76 | 13.69 | 13.43 | 13.17 |

[a] A systematic error of $\sim 0.1$ mag should be applied to the average level of these magnitudes. For the rest, typical errors are $\sim 3\%$.

analogy with the case of AM Her (Szkody, Raymond, and Capps 1982). From this hypothesis with $T = 26,500$ K we obtain a white dwarf radius $R_{WD} = 3.4 \times 10^8 \times (d/1000 \text{ pc})$ cm. The suggested value of the distance, $d \approx 100$ pc, is completely plausible, as discussed by Bailey *et al.* (1983) and in the following. The white dwarf interpretation of the ultraviolet continuum is also consistent with the possibility that some absorption features in the optical spectra of the low state may be Zeeman components of H$\beta$. A difficulty may however be introduced by the absence of a broad Ly$\alpha$ absorption feature, as expected at these temperatures (e.g., Szkody, Raymond, and Capps 1982), which should be clearly visible in the spectrum, in spite of the intense geocoronal Ly$\alpha$ emission.

A composite spectrum obtained combining the ultraviolet observations and the optical photometry in the low state is shown in Figure 7. Magnitudes measured at $\varphi = 0.8$ are reported, which should represent the brightness outside the minimum. It is clear that the emission from the hot white dwarf which can account for the ultraviolet continuum, is well below the fluxes observed at longer wavelengths. Though some variability over the $10^d$ interval between the UV and optical observations cannot be excluded, the continuity between the 3000 Å *IUE* flux and that in the $U$ band indicates that it should not be substantial. The excess emission in the optical-infrared bands could be due to the secondary star and/or to cyclotron emission from a residual accretion column. The available data are

not sufficient to evaluate the two contributions separately; however, one can take them to represent upper limits to the emission from the secondary star. From the Roche lobe filling condition with a mass ratio $0.1 \leq q \leq 1$ its radius should be between $0.15\ R_\odot$ and $0.42\ R_\odot$. For a main-sequence star the corresponding spectral types are M3–M8 with 3000 K $> T > 2400$ K. Fitting the excess emission with blackbodies in this range, gives acceptable distance values between 50 and 200 pc.

In Figure 7 the sum of two blackbody distributions ($T = 26,500$, $T = 3000$ K) is compared with the low state observations. The best fit curve falls somewhat below the measured $B$ and $V$ magnitudes allowing for a contribution from a residual accretion column with $F_\lambda = 5 \times 10^{-16}$ ergs cm$^{-2}$ s$^{-1}$ Å$^{-1}$ at 5500 Å. The modulation observed in the $V, R, I$ bands in the low state could indicate a contribution from the accretion column somewhat higher than this lower limit, implying a contribution from the secondary star smaller than assumed above. Alternatively the modulation in the low state could result from ellipsoidal or heating effects of the secondary. Extensive observations, polarimetry, photometry, and spectroscopy of a future low state are needed in order to evaluate the stellar and cyclotron contributions separately.

### b) High State Continuum

A composite spectrum obtained from the simultaneous UV optical and infrared observations of 1983 April is shown in Figure 8. The fluxes (*crosses*) represent averages over the light curve. Subtracting from these the emission of a white dwarf and of an M5 V secondary as estimated above, the fluxes represented by dots are obtained. The resulting overall distribution is steeper than the original one shortward of 2000 Å and flatter in the 2000–6000 Å range. A rapid falloff at infrared frequencies is also indicated, especially if one considers that the blackbody distribution underestimates the stellar emission in this spectral range.

The change in slope around 2000 Å suggests that two components are present. The steeper one could derive from the Rayleigh-Jeans tail of a hot spot ($T \gtrsim 50,000$ K), possibly associated with a polar cap. A fit of the data shortward of 10,000 Å with two power laws, $F_\lambda = C_1 \lambda^{-4} + C_2 \lambda^{-1}$, gives the result shown in Figure 8. Though the choice of the exponents is not unique, the data are at least consistent with the above suggestion. Simultaneous soft X-ray observations are needed in order to determine the temperature and area of the hot spot.
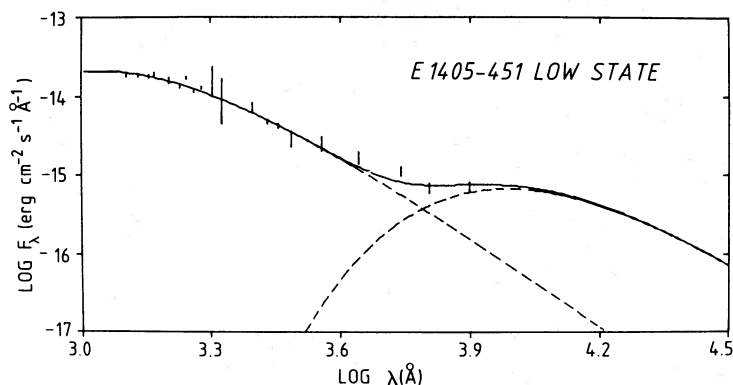


FIG. 7.—Overall energy distribution of E1405−451 in the low state. The bars represent the observations. The continuous curve is the sum of two blackbody distributions with $T = 26,500$ K, $R = 3.4 \times 10^8 \times (d/100 \text{ pc})$ cm, and $T = 3000$ K, $R = 3.8 \times 10^{11} \times (d/100 \text{ pc})$ cm. The dashed curves represent the individual distributions.
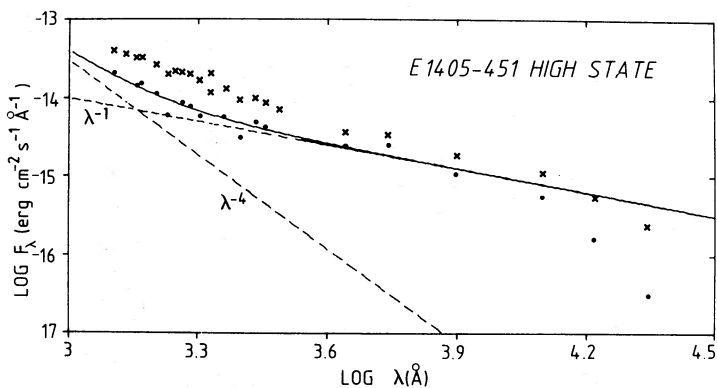
FIG. 8.—Overall energy distribution of E1405−451 during the high state. The crosses represent observed fluxes. The dots are the result of subtracting from the observed fluxes, the contribution of the white dwarf and of the main sequence stars as estimated in Fig. 6a. The continuous curve is the best fit of the dots obtained with the sum of two power laws $F_\lambda \propto \lambda^{-\alpha}$ with fixed spectral indices, $\alpha_1 = 4$ and $\alpha_2 = 1$.

The flatter component $F_\lambda = C_2 \lambda^{-1}$ should derive from thin cyclotron radiation. In fact, the spectral index was chosen in analogy with that of the eclipsed component of AM Her (Raymond *et al.* 1979). The increasing cyclotron optical depth could be responsible for the falloff at infrared frequencies, where the continuum shape is again consistent with a Rayleigh-Jeans distribution.

### c) The Lines

The presence of lines corresponding to different ionization states and with complex profiles indicates that various regions contribute to the emission.

The amplitude and phase of the radial velocity curve of E1405−451 favors the secondary as the emission region of the narrow components of the lines. In fact, in this case the mass function is consistent with the mass of the secondary estimated above (§ IVa), while in the opposite hypothesis, i.e., that the observed velocity is associated with the motion of the white dwarf, an implausibly low mass would result. Moreover, the zero in radial velocity at $\varphi = 0$ is consistent with inferior conjunction of the secondary, which can account for the observed line intensity minimum.

The broad components are usually thought to derive from gas streaming toward the accretion funnel and may differ in velocity both from the narrow components and from the deeper region of the accretion column (cf. Fig. 1 of Liebert and Stockman 1983). The present data are insufficient for a discussion of this component.

The inverted Balmer decrement of both components $F_{H\beta}/F_{H\alpha} = 1$–2, similar to that observed in AM Her, can be interpreted in terms of collisional and opacity effects in a high-density gas ($n \approx 10^{12}$ cm$^{-3}$) (Liebert and Stockman 1983).

In the low state the resonance UV lines and the Balmer lines practically disappear, while the intercombination line O III $\lambda1660$ persists. This can be understood if, due to a decreased accretion rate and far-UV emission, the density in the emission regions is lower than in the high state. Consequently, the very broad C IV emission, possibly present in the low state, could indicate that density conditions suitable to produce the resonance lines are met deeper in the accretion column, where the velocity is larger.

### d) Geometry of the System

In several AM Her–like systems the modulation of the continuum intensity is understood as due to the accretion column

being occulted by the rotating white dwarf. This also corresponds to an inversion of the sign of the circular polarization when the column crosses the limb of the white dwarf. This does not occur in E1405−451 where the circular polarization is always positive (Tapia 1982; Bailey *et al.* 1983).

On this basis Bailey *et al.* (1983) propose a different picture, where at $\varphi = 0$ the column is pointed toward the observer and the modulation is due to intrinsic beaming of the cyclotron radiation outside a cone centered on the magnetic axis. The observed minimum in the circular polarization would be due to dilution of the cyclotron radiation by other sources of light in the system. This interpretation is consistent with the radial velocity curve if the column points toward the companion in azimuth as suggested also for other polars (cf. Liebert and Stockman).

However, this model is questioned by the observations of Tapia (1982) and Visvanathan and Tuohy (1983), which show linear polarization pulses near $\varphi = 0$. Since linear polarization pulses are usually attributed to the column being perpendicular to the line of sight, it is difficult to see how the two pictures can be reconciled.

### V. CONCLUSION

The discovery of a low state in the emission of E1405−451 has enabled us to recognize the emission from a hot white dwarf in the far-ultraviolet region of the spectrum and to estimate the contribution of the secondary star of spectral type later than M3 V, in the optical-infrared bands.

In the high state, besides these two sources of radiation, two components seem to be present. One is a relatively flat distribution, becoming self-absorbed in the infrared, which is likely to be due to cyclotron radiation. A steep component, consistent with a Rayleigh-Jeans distribution between 1000 and 2000 Å, suggests the presence of a hot spot at the polar cap, analogous to that hypothesized in other polars. A confirmation of the existence of this component and a determination of its temperature and extension require soft X-ray observations simultaneous with the ultraviolet ones.

## REFERENCES

Angel, J. 1977, *Ap. J.*, **216**, 1.
Bailey, J., *et al.* 1983, *M.N.R.A.S.*, **205**, 1.
Blades, J. C., and Cassatella, A. 1982, *IUE* ESA Newsletter, No. 17, p. 12.
Bohlin, R., and Holm, A. 1981, *IUE* ESA Newsletter, No. 11, p. 18.
Chiappetti, L., Tanzi, E. G., and Treves, A. 1980, *Space Sci. Rev.*, **27**, 3.
Cowley, A. P., and Crampton, D. 1977, *Ap. J. (Letters)*, **212**, L121.
Jensen, K. A., Nousek, J. A., and Nugent, J. J. 1982, *Ap. J.*, **261**, 625.
Liebert, J., and Stockman, H. S. 1983, in *Cataclysmic Variables and Low Mass X-ray Binaries*, eds. J. Patterson and D. Q. Lamb (Dordrecht: Reidel).
Mason, K. O., *et al.* 1983, *Ap. J.*, **264**, 575.

Nousek, J. A., and Pravdo, S. H. 1983, *Ap. J. (Letters)*, **266**, L39.
Paczyński, B. 1971, *Ann. Rev. Astr. Ap.*, **9**, 183.
Raymond, J. C., Black, J. H., Davis, R. J., Dupree, A. K., Gursky, H., Hartmann, L., and Matilsky, T. A. 1979, *Ap. J. (Letters)*, **230**, L95.
Schmidt, G. D., Stockman, H. S., and Margon, B. 1981, *Ap. J. (Letters)*, **243**, L157.
Szkody, P., Raymond, J. C., and Capps, R. 1982, *Ap. J.*, **257**, 686.
Tapia, S. 1982, *IAU Circ.*, No. 3685.
Visvanathan, N., and Tuohy, I. 1983, *Ap. J.*, **275**, 709.
Wickramasinghe, D. T. 1982, *Proc. ASA*, **464**, 328.

J. M. Bonnet Bidaud: CEN Saclay, DPh-EP/SAp, B.P.2, 91190 Gif-sur-Yvette, France

A. Lauberts: European Southern Observatory, Karl Schwarzschild-Str. 2, D 8046 Garching bei München, West Germany

L. Maraschi and A. Treves: Dipartimento di Fisica, Universitá degli Studi, Via Celoria 16, 20133 Milano, Italy

C. Motch: Observatoire de Besançon 41 bis, Av. de l'Observatoire 2500 Besançon, France

M. Mouchet: Observatoire de Paris, 92190 Meudon, France

M. M. Phillips: Observatorio Interamericano de Cerro Tololo, Casilla 603, La Serena, Chile

E. G. Tanzi: Istituto di Fisica Cosmica del CNR, Via Bassini, 15, 20133 Milano, Italy